UNSTEADY SIMULATION OF THE LP TURBINE TEST CASE T106D-EIZ USING A TRANSPORT EQUATION BASED TRANSITION MODEL

F.Blaim and R.Niehuis
Institut für Strahlantriebe der Universität der Bundeswehr München

Abstract

This paper gives an overview of the capabilities for unsteady flow simulations of low pressure turbine cascades by using modern transition models. The numerical results are compared to the experimental test case T106D-EIZ measured at the high-speed test facility of the University of German Armed Forces Munich. The T106D-EIZ is an ultra-high-lift profile with a pitch to chord ratio of 1.05 and therefore has a big separation bubble even at a high Reynolds number. Many transition models are calibrated with the moderately loaded (pitch to chord ratio of 0.799) T106A test case, which makes the T106D-EIZ a very demanding test case for the prediction capabilities of modern transition models using the Unsteady Reynolds Averaged Navier Stokes (URANS) equations. A special focus lies on the comparison between the different correlations proposed by Menter and Malan for the $\gamma - Re_{\theta t}$ local quantities transport transition model. Both correlations are compared to the experimental results and results obtained by a transition model relying on integrated boundary layer parameters. In a first step the results of the steady test case situation are analysed to calibrate the correct axial velocity density ratio for the quasi 3D calculation. After that time averaged isentropic Mach number distributions, obtained by unsteady flow simulations, are analysed to highlight the differences between the different transition models. This also includes comparisons of time space distributions of the quasi wall shear stress rate with computed shear stress rate. Especially in that analysis larger differences were found, which could not be explained using the conventional time space diagram. Therefore, a 3D time space diagram was used to highlight the differences within the local quantities used by the $\gamma - Re_{\theta t}$ transition model. This analysis lead to a proposal in which way this model could be improved to gain better prediction capabilities.

1. NOMENCLATURE

MODEL CONSTANTS

$A_l = 10$ $B_l = 20$

$C_l = 30$ $D_l = 40$

$E_l = 50$ $F_l = 60$

$G_l = 70$ $H_l = 80$

$I_l = 90$

$A_{\theta C} = 10$ $B_{\theta C} = 20$

$C_{\theta C} = 30$ $D_{\theta C} = 40$

$E_{\theta C} = 50$ $F_{\theta C} = 60$

$G_{\theta C} = 70$

SYMBOLS / ABBREVIATIONS

AVDR	Axial Velocity Density Ratio
c_f	friction coefficient $c_f = \frac{\tau_w}{\frac{1}{2}\cdot\rho\cdot c_\infty{}^2}$
c	fluid velocity
d	diameter
d_w	distance from wall in normal direction to wall
Dif	diffusion term in a transport equation
EIZ	unsteady Wake Generator
F_{length}	transition length parameter
Ma	Mach number
QWSS	quasi wall shear stress
Re_θ	momentum thickness Reynolds number
$Re_{\theta t}$	momentum thickness Reynolds number at which laminar transition occurs.
δRe_θ	difference $Re_{\theta C} - Re_{\theta t}$
ρ	fluid density
t	pitch
t/T	time normalized by bar passing period T
τ_w	wall shear stress
γ	intermittency
y^+	nondimensionalized wall distance

SUBSCRIPTS

ax	axial quantity
b	quantity related to the moving bar
c	related onto the blade chord
C	critical quantity
Mal	Malan correlation parameter
Dest	destruction term
Prod	production term
is	isentropic quantity
x	component in x direction
∞	frestream quantity observed at the boundary layer edge

2. INTRODUCTION

The transition between laminar and turbulent flow is the most important loss determining effect in turbines. Many approaches were made to model this physical region. The most important work for the understanding of the correlation based modeling was made by Mayle [1]. These correlations are based on the boundary layer parameters described by Schlichting [2]. To implement a valid transition model into an established flow solver, test cases are required providing most of the relevant effects, which should be captured by the models. The T106D-EIZ aerodynamic fulfills this requirement because it has a high

aerodynamic blade loading forcing flow separation and laminar to turbulent transition on the suction surface. The test case was first published by Stadtmüller [3]. In many cases the ERCOFTAC flat plate test cases are used to demonstrate that the implemented transition models are valid, but most models perform very well under these aseptic flow conditions without considering more complex effects like curvature and unsteadiness of real-life test cases shown by Kelterer et al. [4]. Therefore, it is absolutely necessary to validate transition models on complex test cases. Right now there are implemented two transition models in the TRACE simulation framework used within this study, the so-called multimode transition model by Kožulović [5] and the γ-$Re_{\theta t}$ model based on Menter´s [6,7] description. This model also supports the correlations published by Malan [8]. It is the main objective of this paper to compare and assess the different transition models by using the ultra-high lift T106D-EIZ test case showing the differences especially generated in the separating part of the suction side. After highlighting differences between experimental and numerical results, the reason for the observed differences are ascertained and a proposal for necessary improvements relying on the T106D-EIZ test case is made.

3. TEST CASE DESCRIPTION

The T106D-EIZ was part of the joint research program “Periodisch Instationäre Strömungen in Turbomaschinen” of the Deutsche Forschungsgemeinschaft (DFG), aiming at the ultra-high lift turbine-blading design philosophy to reduce the overall weight of the turbine component

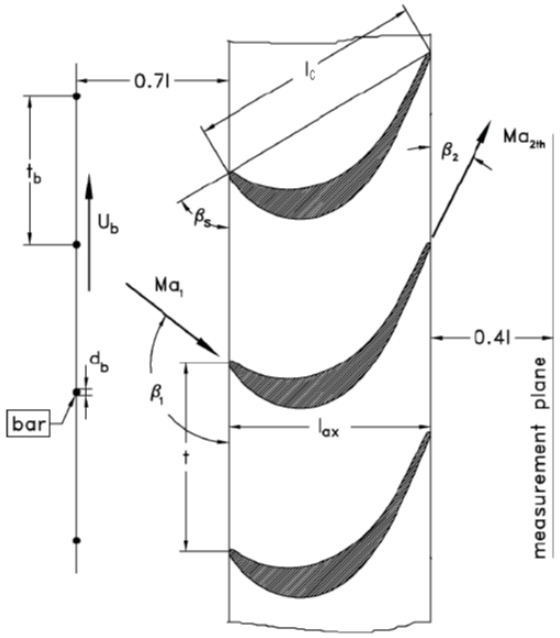

Figure 1 T106D-EIZ test case setup

maintaining high efficiencies by using unsteady wake passing effects to stabilize the boundary layer. The wakes were generated by using the so-called “Erzeuger Instationärer Zuströmung” (EIZ). The used profile was generated by taking the geometry of the well investigated T106A low pressure turbine airfoil and expanding the pitch to chord ratio from 0.799 to 1.05. This generated an ultra-high lift loaded profile leading in case of steady homogeneous inflow conditions to a big separation even at a high Reynolds number of 200.000. The profile geometry is shown in figure 1 and the main profile parameters are given in Table 1. This behavior should enable to investigate the unsteady transition process in high detail. To deliver a good basis for numerical investigations this test case also contains measurements of unsteady inflow conditions $0.4\,l_c$ upstream of the cascade. In order to obtain the time-resolved development of the boundary layer hot film measurements were performed on the blade surfaces. For all other measurements e.g. the isentropic Mach number (Ma_{is}) distribution standardized measurement techniques were used.

4. NUMERICAL METHOD

The flow solver TRACE developed by DLR Cologne and MTU Aero Engines is a Rieman based code, which solves the Unsteady Reynolds Averaged Navier Stokes equations (URANS). It also has a limiter based on Roe which provides higher stability for the URANS equation system. For time discretization the Crank-Nicholson time discretization scheme [9] combined with the pseudo time approach based on Jameson [10] is used. Two different stagnation point anomaly fixes can be used, one following the description by Kato and Launder, see [11], and the other is following the description of Durbin and Peterson Reif [12], for both see [13]. For more details on the TRACE code it is refered to [14],[15].

4.1. Multimode Transition Model

The multimode transition model was implemented by Kožulović [5],[16]. It is an integrative approach using the correlations found by Mayle [1]. This approach requires a structured mesh around the surfaces on which transition may occur. It is also important that the entire boundary

Operating Conditions and Geometry of the Cascade	
Theoretical Exit Reynolds number	$Re_{2th} = 200.000$
Theoretical exit Mach number	$Ma_{2th} = 0.59$
Geometric inflow angle	$\beta_1 = 127.7°$
Inflow turbulence intensity	$Tu = 2.5\%$
Stagger angle	$\beta_S = 59.28°$
Chord length	$l_c = 100mm$
Blade pitch	$t = 105mm$
Bar velocity $Re_{2th} = 200.000$	$U_b = 21.4\,\frac{m}{s}$
Bar pitch	$t_b = 40mm$
Bar diameter	$d_h = 2mm$

Table 1 Test case parameters

layer is lying within one block because the numerical solution method does not allow for the integration over two different block boundaries. After the integrated boundary-layer parameters are found (displacement thickness δ_1 and momentum thickness θ), they are used to determine a numerical intermittency factor. This intermittency is used to couple the $k-\omega$ equations with the transition model as shown in eq. (1) and (2),see [5].

$$(1)\qquad \frac{\partial(\rho k)}{\partial t}+\frac{(\rho U_i k)}{\partial x_i}=\gamma_{Prod}P_k-\gamma_{Dest}\cdot D_k+Dif_k$$

$$(2)\qquad \frac{\partial(\rho \omega)}{\partial t}+\frac{\partial(\rho U_i \omega)}{\partial x_i}=\gamma_{Prod}\cdot P_\omega-\gamma_{Dest}\cdot D_\omega+Dif_\omega$$

4.2. Gamma Reynolds theta Model

The $\gamma-Re_{\theta t}$ Model was first introduced by Menter [6,7]. It adds two transport equations to the flow solver, one used for the intermittency γ and the second equation for the transition Reynolds number ($Re_{\theta t}$) based on the momentum thickness. $Re_{\theta t}$ denotes the momentum Reynolds number at the position of transition onset in the flow field. Although this boundary parameter is based on the integration over the boundary layer thickness, resulting in a 1-D quantity, it can nevertheless be used to

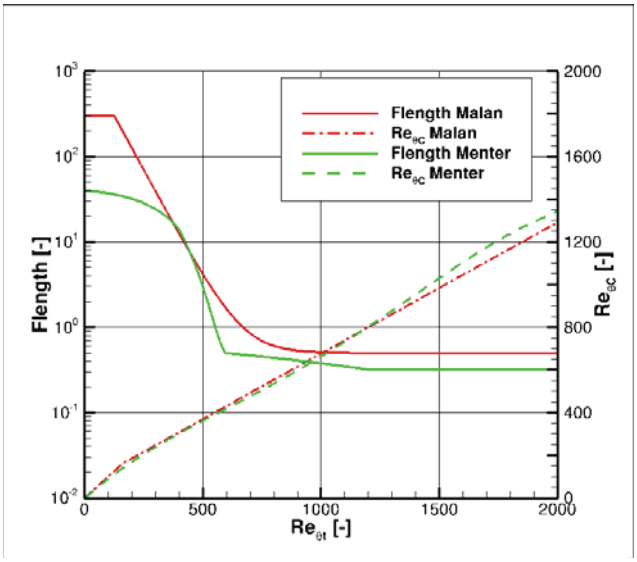

Figure 2 Comparison of the Correlations by Menter and Malan

characterize a 3D flow field [17]. The γ-$Re_{\theta t}$ transition model was meant by Menter as a modeling framework to allow for different correlations easily implemented into this framework. The most influential parameters are the critical momentum thickness Reynolds number $Re_{\theta C}$ and the transition zone length control parameter F_{length}. Both parameters are empirically correlated to $Re_{\theta t}$. $Re_{\theta C}$ represents the critical momentum thickness Reynolds number at which the intermittency starts to grow. The F_{length} parameter is used to weight the production term within the intermittency equations. For sometime Menter did not publish these essential correlations for proprietary reasons. It was Malan [8] who described and published his own correlations. These are given here in eq. (3). This gave motivation to Menter to publish his correlations, too [18].

$$(3)\qquad \begin{aligned} Re_{\theta cMal} &= \min(0.615\cdot Re_{\theta t}+61.5, Re_{\theta t}) \\ F_{lengthMal} &= \min(\exp(7.168-0.01173\cdot Re_{\theta t})+0.53, 300) \end{aligned}$$

The correlation by Menter is a little bit more complicated as shown in eq. (4), see [18].

$$(4)\qquad F_{length}=\begin{cases} [A_l+B_l Re_{\theta t}+C_l\cdot Re^2_{\theta t}] & Re_{\theta t}<400 \\ [D_l+E_l\cdot Re_{\theta t}+F_l\cdot Re^2_{\theta t} & 400\le Re_{\theta t}<596 \\ \quad +G_l\cdot Re^3_{\theta t}] & \\ [H_l-(Re_{\theta t}-I_l)\cdot 3.0\cdot 10^{-4}] & 596\le Re_{\theta t}<1200 \\ [0.3188] & 1200\le Re_{\theta t} \end{cases}$$

$$R_{\theta c}=\begin{cases} [Re_{\theta t}-A_{\theta C}+B_{\theta C}\cdot Re_{\theta t} & \\ \quad +C_{\theta C}\cdot Re^2_{\theta t}+D_{\theta C}\cdot Re^3_{\theta t} & \\ \quad +E_{\theta C}\cdot Re^4_{\theta t} & Re_{\theta t}\le 1870 \\ [Re_{\theta t}-(F_{\theta C}+(Re_{\theta t}-G_{\theta C})\cdot 0.482)] & Re_{\theta t}>1870 \end{cases}$$

In [4] the differences between these two correlations were shown for the steady simulation of the T106A test case. Therefore, differences can also be expected for unsteady simulations of the higher loaded test case T106D-EIZ. The most significant difference between the two correlations sets are depicted in figure 2. As can clearly be seen the most significant difference is found for the distribution of the parameter F_{length}. The critical Reynolds number referenced to the momentum thickness $Re_{\theta C}$ shows only small differences between the two parameter sets.

5. NUMERICAL SETUP

In this part of the paper the numerical setup including the computational mesh and its size, the boundary conditions, and the generated results will be described and discussed.

5.1. Computational Mesh

For the computations an OCGH structured grid was used generated by the high quality mesh generator G3DHexa developed by DLR Cologne and MTU Aero Engines. The O-block around the suction side blade surface consists of 6497 cells and was merged with the C block of 2090 cells to enable the integration for the multimode transition model. To take secondary flow phenomena into account, which lead to a higher velocity in the accelerating part of the profile, an AVDR ratio of 0.93 as proposed by Schwarze et al.[19] was applied by making the stream-

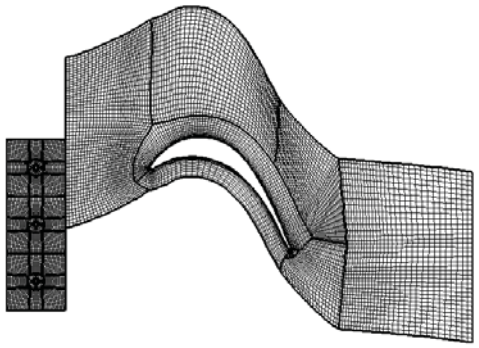

Figure 3 Computational domain showing only every second nodal point.

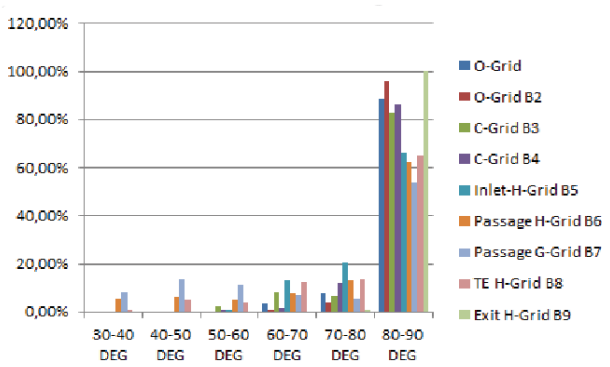

Figure 4 Edge angle distribution for the different mesh blocks

tube ,consisting of 1 cell layer, linearly wider between leading edge and trailing edge. This leads to a higher acceleration in the part before the maximum of the isentropic Mach number. The mesh is shown in figure 3 and consists out of 9 blocks. Within the O-block around the blade 31 points in the nearly perpendicular direction to the blade-surface are provided generating a high resolution mesh, which delivers a non-dimensionalized wall distance y^+ at the blade surface well below 1. 209 points are used for the suction side, i.e. in total 319 points around the complete bladesurface, which provide a good discretization for the sensitive transition region. Therefore the computational mesh is capable to resolve the transitional effects within the viscous sublayer.

A percentaged distribution for the cascade cell vertex angles is shown in figure 4 and it can be seen that only a small fraction of cells (2.35%) show not so good, but still acceptable angles in the range of 30-40 degrees. For the steady homogeneous inflow case a mesh sensitivity study was undertaken and showed good results for this mesh. The bar mesh for the unsteady rotor simulation consists of three equally meshed bars with a diameter of 2 mm. Those segments consist of one O-grid, containing 2178 cells, enclosed by eight H-grids leading to an overall cell count of 6470. To simulate the translation of the bars this complete mesh was transformed onto a 50 meter radius to enable rotational movements of the bar mesh. The complete mesh is displayed by plotting only every second nodal point in figure 3. The bar pitch was reduced from 0.04m by 12.5 percent to 0.035m in order to obtain an integer multiple with the cascade pitch.

5.2. Boundary Conditions

The moving bars were coupled by a sliding mesh interface to the turbine cascade mesh at a distance of $0.4 l_{ax}$ away from the leading edge. This interface is also capable to interpolate the primitive variables between structured and unstructured mesh partitions, see [20],[21]. Although it was first developed for the structured use only [22]. For the hub and tip of the domain adiabatic free-slip boundary conditions were applied. For all other walls no-slip adiabatic boundary conditions were applied. The multimode transition model was turned on, only at the walls of the suction side at the cascade. For the outlet boundary condition the pressure of the original test case measurements was applied to a non-reflecting Fourier boundary condition. The inlet boundary condition consists of a Fourier boundary condition formulation, which can deal with the potential effects leading to a fluctuating pressure at the inlet boundary plane. The inlet boundary condition fixes the averaged stagnation pressure to the measured stagnation value given in the test case description of the T106D-EIZ [23].

The most important condition for the correct simulation of the transition process near the cascade profile is the turbulent length scale. In this case a turbulent length-scale of $5*10^{-5}$m was chosen, this resulted in an inlet turbulent viscosity ratio of about 3.5 similar to that obtained by Schwarze et al. [19]. One passing of a segment of three bars was resolved with 1600 time-steps, resulting in a time-step size of $3.28125*10^{-6}$s

5.3. Investigated Cases

For being able to compare the $\gamma - Re_{\theta t}$ model against the integration based multimode transition model only the higher Reynolds number of $2.0 \cdot 10^5$ was investigated here. This operation condition will lead to a reattachment of the separated flow and is therefore a good test case for both transition models. Both models were investigated for a Mach number of 0.59 using the bar configuration with a bar pitch of 0.035m. For the multimode transition model a stagnation point anomaly fix following the procedure by Schwartz was used, see [12]. This setting was chosen to be consistent with the published results by Schwarze et al. [19]. For the $\gamma - Re_{\theta t}$ transition model the stagnation point anomaly fix described by Kato Launder was used, this model is especially calibrated for this treatment of the overproduction of kinetic energy. But those cases were also investigated by using the Schwartz limiter, however, it turned out with that limiter no laminar separation bubble could be obtained.

6. RESULTS

After summarizing the results for steady inflow conditions the further analysis will concentrate on unsteady inflow conditions. The results will be compared to experimental data followed by a detailed analysis of the temporal boundary layer development on the suction surface.

6.1. Steady Inflow

Similar to the 2D steady flow simulations it is expected that secondary flow phenomena do influence the flow at midspan of the blade in case of unsteady inflow conditions. In this case the channel height has to be reduced from 300 mm to 176 mm due to the installation of the wake generator. Therefore a carefully choice of a suitable AVDR is essential. This procedure was performed by using test data obtained for test runs at reduced channel height and wake generator installed, but without running the wake generator and no bars installed. With installed EIZ also the inflow angle changes compared to the steady configuration due to leakage flow near the moving bar belt, which generates a deviation of the airflow direction. Therefore, a variation of both the inflow and the AVDR must be considered. This can be very expensive in terms of computational time in case of an unsteady variation. For this reason, the steady experimental results for the wake generator configuration were compared against the simulated results using an AVDR of 0.93 and a positive incidence of two degrees leading to an aerodynamic inflow angle of 129.7°. This configuration was proposed by Schwarze et al. [19], and is proved as a valid

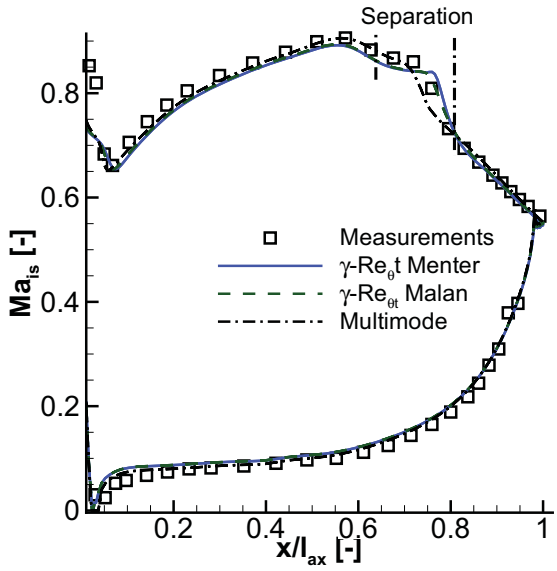

Figure 5 Computed isentropic Mach number distributions for the three different transition models

configuration, see figure 5. The first separation near the leading edge is captured very well by all three transition models. At about $0.1\,x/l_{ax}$ the relaminarization starts by the strong acceleration on the suction surface, see figure 5. All three models deliver good results for the pressure distribution showing a big separation bubble starting at about $0.7\,x/l_{ax}$ and ending with a reattached flow at $0.8\,x/l_{ax}$. Even though all three transition models predict the main effects for the separation bubble, differences can be observed by a closer look. Compared to the reference multimode transition model, the $\gamma-Re_{\theta t}$ model using correlations by Malan shows a lower tendency to separate than the $\gamma-Re_{\theta t}$ transition model using the correlations by Menter. At this point of the analysis the correlations by Malan seem to outperform the correlations by Menter for

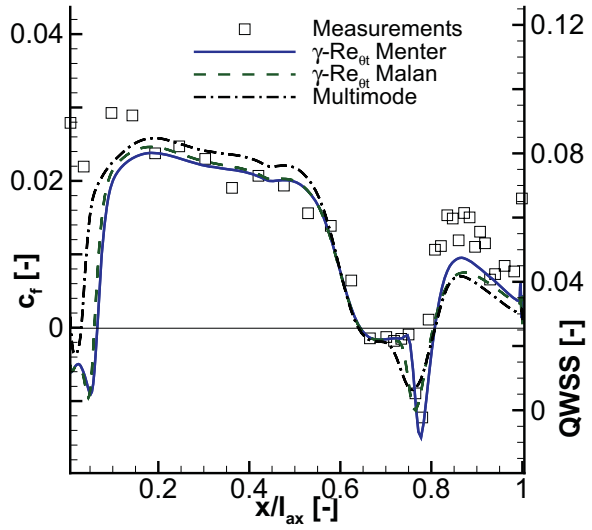

Figure 6 Showing the measured quasi wall shear stress compared to the calculated results of the different transition models

an ultra-high lift profile. But this cannot be affirmed by comparing the quasi wall shear stress QWSS, generated by hot film data, to the friction coefficient of the calculations as depicted in figure 6. It has to be noted that the quasi wall shear stress was not calibrated and therefore the values were approximated by overlaying the acceleration part of the c_f values with the quasi wall shear stress in that region. This leads to a determination of the starting point of the separation, which aligns very well with the computed data. After the reattachment, the c_f values did not increase as much as the quasi wall shear stress measured in the experiment. But the overall prediction quality for the steady case can be considered as very good. In a next step the analysis will be concentrated on unsteady inflow conditions.

6.2. Unsteady Inflow

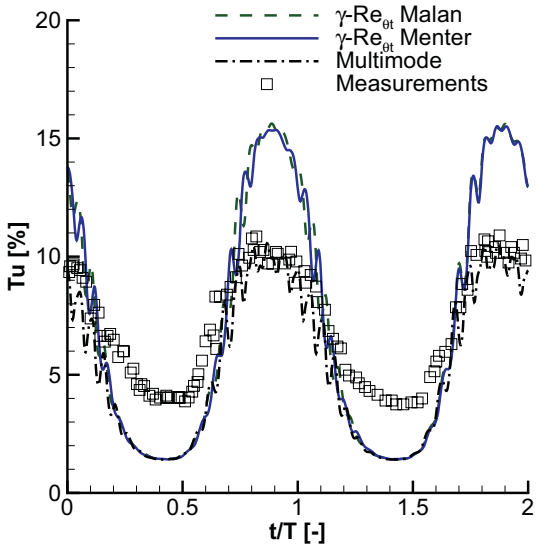

Figure 7 Wake turbulence levels $0.4\ x/l_{ax}$ upstream of the cascade

In order to simulate the unsteady interaction between the wakes generated by the EIZ and the cascade a good simulation of the wakes generated by the bars is crucial. Therefore, the numerical results are compared to experimental data in an inlet plane between the wake generator and the cascade. A time dependent signal (turbulent kinetic energy velocity and pressure) was taken from the CFD results by an artificial probe located at $0.4{\cdot}x/l_{ax}$ upstream of the leading edge. The probe location is shown in figure 8a).

The distributions of turbulence intensity in that plane are compared to the measured results in Figure 7. The multimode model was applied only on the suction surface of the cascade. But the $\gamma-Re_{\theta t}$ was applied to the entire computational domain, resulting in a 5% higher turbulence level in the bar wake .compared to the multimode results without transition modeling applied on the bar surface.

The pressure data was processed by a fast Fourier transformation using a Hamming window into a frequency and corresponding amplitude of the signal. This frequency spectrum exhibits the theoretical bar wake frequency as well as the bar wake passing frequency (600Hz) and its higher harmonics (1200Hz and 2400Hz) figure 8b). The theoretical bar wake frequency can be estimated by

considering the absolute inflow velocity, which is about 120 m/s, the bar diameter of 0.002 m and a Strouhal number of 0.215 as proposed by [2].

(5) $$Sr = \frac{f \cdot d_{bar}}{c}$$

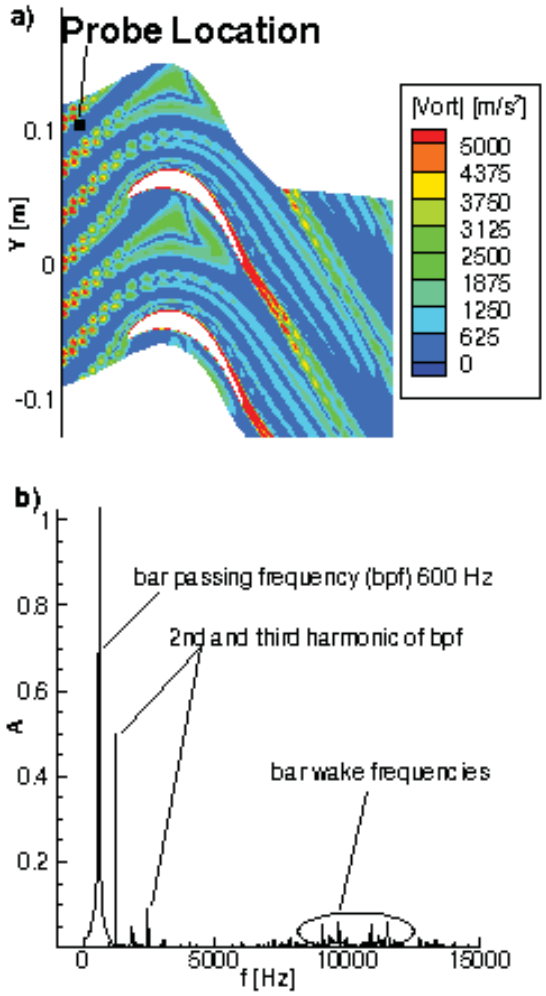

Figure 8 Absolute voritcity contour levels a) and FFT of transient pressure signal b) at the depicted probe location in a).

Using eq. (5), this leads to a theoretical frequency of 12 kHz. This frequency can also be seen in figure 8b). Figure 8a) also shows the von Kármán vortex street visualized by the absolute value of the vorticity. Because both the turbulence level and the spectral frequency analysis show a qualitatively good agreement between measured and theoretical data it can be concluded that the bar wake kinematics is predicted precisely enough allowing to study the impact of the wake on the boundary layer of the cascade in detail.

6.3. Unsteady Boundary Layer Development

The time averaged Ma_{is} distributions are depicted in figure 9 and compared to the experimental data. It can clearly be seen that all the three transition models are not

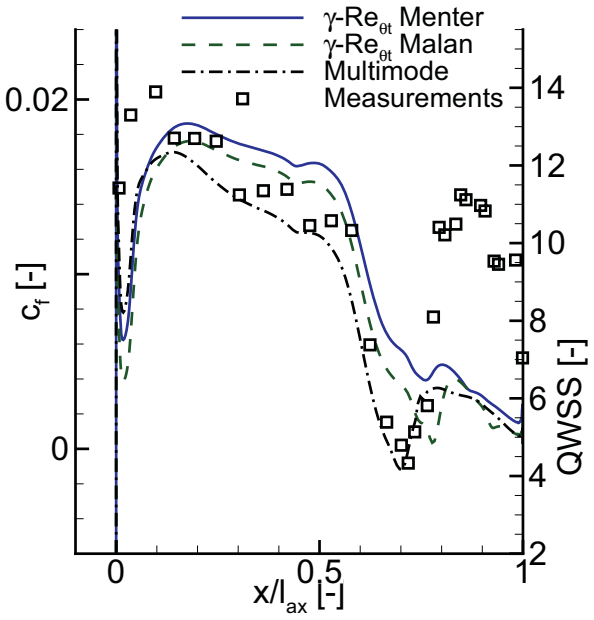

Figure 10 Time averaged skin friction coefficient compared against measured quasi wall shear stress

able to predict the flow separation on the suction surface correctly. The best prediction is delivered by the multimode transition model. The time averaged data show significant differences between the three different transition models. These can better be illustrated by comparing computed skin friction coefficient values and measured quasi wall shear stress, see figure 10. It is obvious, that the multimode transition model better predicts the experimental data compared to the $\gamma - Re_{\theta t}$ model looking e.g. at transition onset location and the location of the separation bubble. It also depicts that the location of the separation bubble calculated with the multimode transition model shows a good agreement to the measured location.

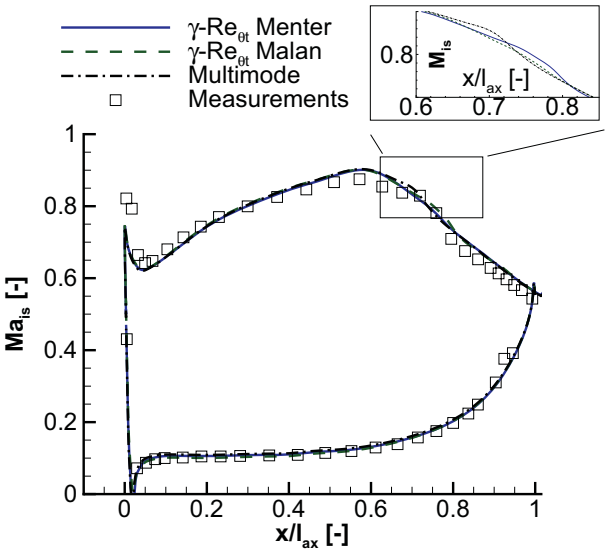

Figure 9 Time averaged isentropic Mach number distribution

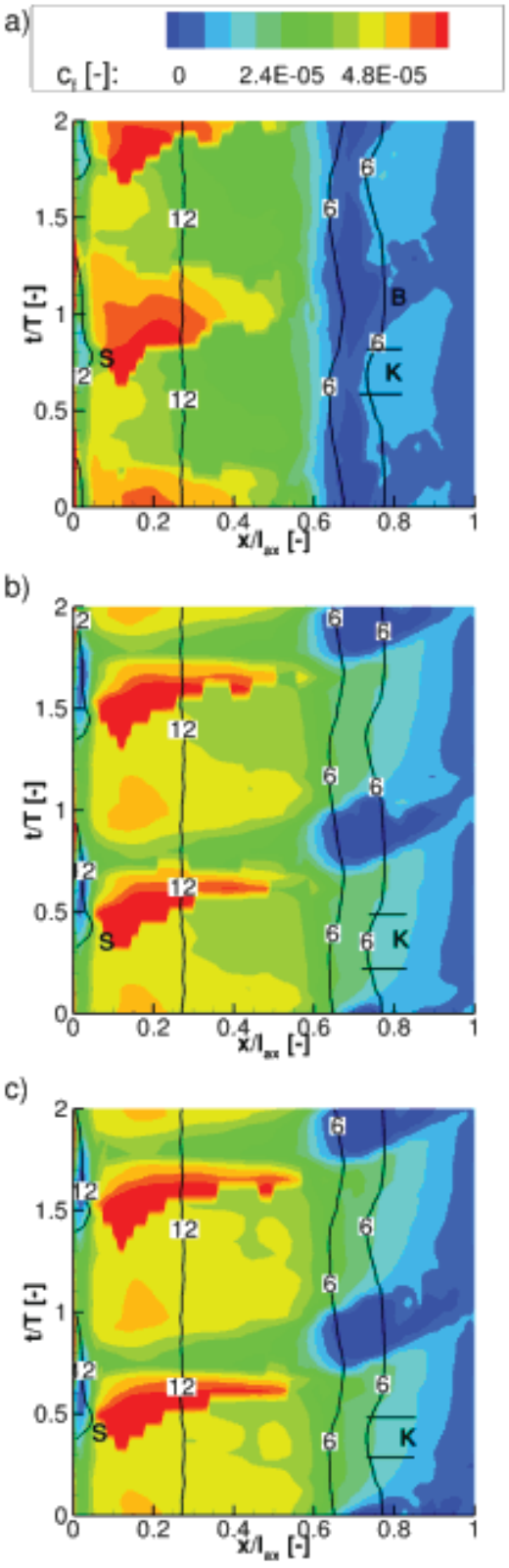

Figure 11 skin friction coefficient for multimode a) Menter b) Malan c) compared with isolines of quasi wall shear stress with values 6 and 12 near leading edge

The differences between measured data and results computed by the $\gamma - Re_{\theta t}$ models are in contrast to the ability of the $\gamma - Re_{\theta t}$ transition model to correctly calculate the transition location in case of steady inflow condition as shown earlier. Consequently a detailed analysis of the reasons for this difference has to be performed.In order to gain a better understanding of the prediction deficit, the boundary layer development is illustrated by time space diagrams of the friction coefficient c_f in figure 11. The first plot a) shows c_f contours computed by the multimode transition model, compared with the quasi wall stress measured by the hot film sensors on the blade surface. To synchronize the time-steps of the calculations with the measured time step contour values, the value $c_f = 2.4 * 10^{-5}$ was used to adapt contour quasi wall shear stress data of isolevel 12 near the leading edge. Even if the regions vary in time, the measured lines are much longer in time than the computed contour values, characteristic spikes (for the iso line of measured data at position marked with S in figure 11a)) can be seen in both cases. This spike was used to adapt both contours qualitatively in time direction. It can be seen that the main separation bubble, represented by c_f values below zero, is within the range given by the measured bands between 0.7 and $0.8\,x/l_{ax}$. The becalmed region can be identified clearly in a widening of the separation bubble marked with B in figure 11a). The region with the highest influence generated by the wake can be seen at about 0.6 t/T for both computed and measured data. In the measured data, the wake generates a kink (marked K) within the bands of the quasi wall stress equal 6. In general the results generated with the multimode transition model turn out to agree very well with the measured data. In comparison with the results of the integrative based multimode transition model, both results generated by the use of the $\gamma - Re_{\theta t}$ transition model show significant differences to the measured quasi wall shear stress.

First of all, both show differences in the temporal elongation of the nearly separated flow at the leading edge, but compared to the multimode transition model both correlations (Menter represented by b) and Malan by c)) show much lower levels of c_f at the leading edge of the blade. But this could also be an effect of the Kato-Launder stagnation point anomaly fix used for the $\gamma - Re_{\theta t}$ transition model computations. Due to the fact that it was not possible to detect a distinct spike in the c_f distribution, the measured data were aligned in an suitable temporal range to discuss the computed results of the separation bubble between 0.6 and 0.9 x/l_{ax}. For both $\gamma - Re_{\theta t}$ correlations the temporal length of the separation region is much smaller than in the case of the multimode transition model. This is in line with the flow separation within the time averaged flow data. For both models, however, the separation is temporarily elongated much more over the blade length extending to a point of about $0.9\,x/l_{ax}$.

This is the reason for delayed separation observed by the time-averaged Ma_{is} distribution, cf. figure 9. Between the correlation of Malan and Menter a major difference can be identified within the elongation of the separated region on the blade surface. This elongation seems to be typical for the $\gamma - Re_{\theta t}$ transition model formulation, but is especially overweigthed within the formulation of Malan. From this point of view it seems that the correlation set used by Menter generates slightly better results than the correlation set defined by Malan. In order to analyse the differences between both correlation sets in a better way, the transported local variables must be analysed to

obtain an understanding for the time dependent transportation of the influence factor on the $Re_{\theta t}$ and γ equation sets. This analysis cannot be performed with a conventional time space diagram in 2D, because only the results of the equation on the first cell layer can be visualized. But those results clearly depend upon the transported variables outside the boundary layer. Therefore the complete boundary layer needs to be visualized over the time.

6.4. 3D Time Space Boundary Layer Diagrams

The 3D time space diagram consists of the cell values extracted around the suction side O-block. The distance of a cell from the solid surface is denoted as d_w and is measured as the shortest distance between the cell center and the solid boundary surface. This coordinate is used as z coordinate, by using the x/l_{ax} as value in y direction and again using the normalized time referenced onto the period of a bar passing for x direction, the time dependence of the values within the suction side O-block can be visualized.

An isocontour representing velocity $c_x = 0$ has been used to capture the separation bubble within all 3D time space diagrams as shown in figure 12 and figure 13. Because of the different inflow turbulence values generated by the three different transition models it is necessary to check if the turbulence levels in front of the separation bubble are at the same level. As depicted in figure 12 the turbulence levels in front of the separation bubble at a position of $x/l_{ax} = 0.5$ show major differences between the results generated with the multimode transition model and the $\gamma - Re_{\theta t}$ transition model with correlations by Malan. The results for the Menter correlations were not shown, because those are almost the same as the Malan results. It can be seen by figure 12 that the turbulence levels in the near wall boundary show higher values for the results by Malan than in case of the multimode model. In contrast to the near wall region the other levels within the Malan results show lower values for the turbulence as it is the case for the multimode results. From this it can be concluded that the difference in the wake peak turbulence values as depicted in figure 7 may influence the results leading to an earlier transition within the $\gamma - Re_{\theta t}$ model. To analyse the differences between the two $\gamma - Re_{\theta t}$ transition models, transport values have to be reconsidered.

But before looking closer to this, the numerical intermittency γ within the first cell region of the suction side will be illustrated by figure 13. It can be seen that the Menter correlations generate a higher base level for γ than the Malan correlations. It is also apparent that the Malan correlations generate a higher sensitivity in terms of γ values as the Menter correlations. This is supposed to be one reason for the bigger elongation of the separation bubble downstream a position of $x/l_{ax} = 0.85$ as seen in the Malan computations, cf. figure 13. But the problem with the underestimated temporal elongation of the separation bubble cannot be explained by the different contour plots of γ within the viscous sub-layer.

The main influence parameter for triggering the start of γ production and therefore determining the end of a laminar region is the critical Reynolds number based on the momentum thickness $Re_{\theta C}$. If $Re_{\theta C}$ is smaller than $Re_{\theta t}$ the intermittence production is enhanced. Being strongly dependent on $Re_{\theta t}$ the difference between these two parameters , denoted by δRe_θ can be seen as the main criteria on influencing the starting of the transition process by increasing the γ production. In case of large values for

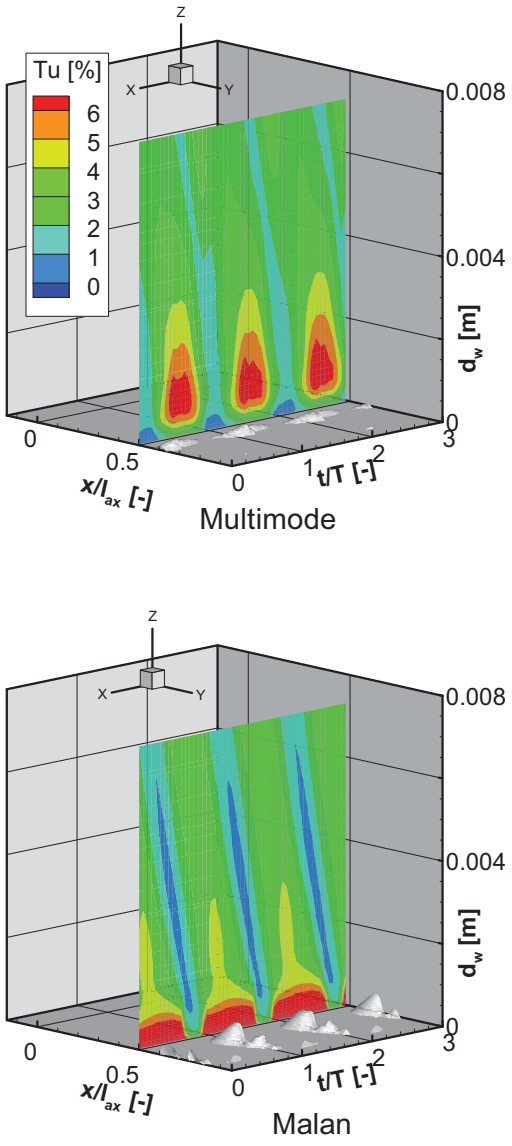

Figure 12 3D Time space diagram of turbulence at $0.5\ x/l_{ax}$.

the δRe_θ the γ production is kept low, in case of zero or negative values, the γ production increases. In figure 13 a cutting plane slightly upstream of the separation bubble displays the δRe_θ values, in order to visualize the impact of the temporal variation of this value on the separation bubble.

For both models a clear increase of δRe_θ can be seen some time before the separation bubble starts to appear. Just before the separation bubble starts to diminish the δRe_θ value reaches zero and triggers higher γ production. Again the correlation set by Menter shows higher values near the surface than in comparison to the correlation set by Malan as depicted in figure 13a). The low values of δRe_θ are highly present within the wake traveling path starting at time $t/T = 1$ at a position $d_w = 0.1$ (marked as A) going to a time $t/T = 1.5$ reaching the near wall region of $d_w = 0.02$ (marked B). Therefore turbulence in the wake seems to influence δRe_θ in an unfavorable way causing the predicted separation bubble for both cases to be underestimated in terms of its temporal extension. A

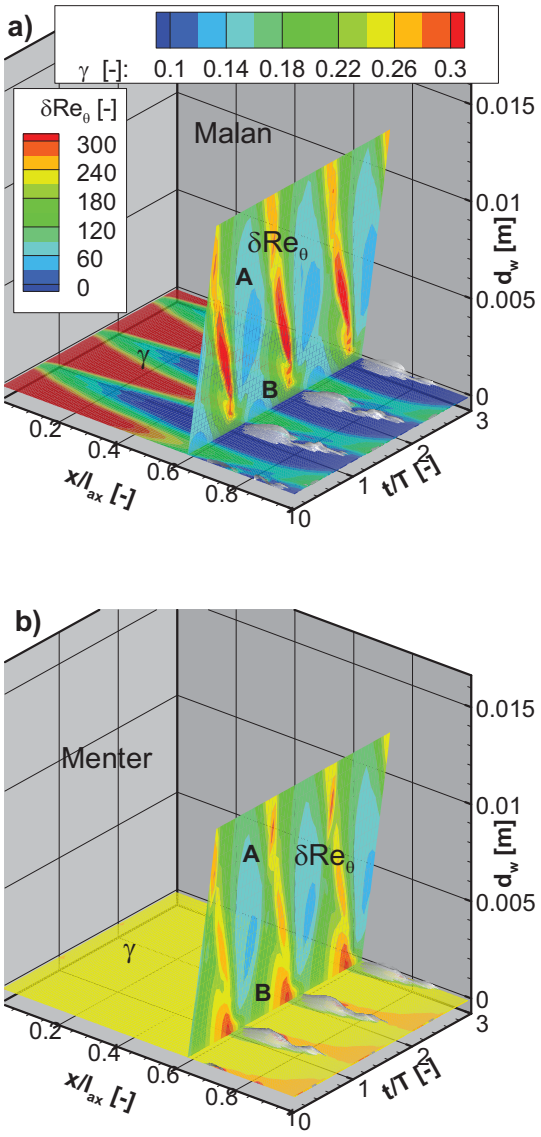

Figure 13 3D time space diagrams a) showing influence parameters for the Malan correlation set. b) influence parameters for the Menter correlation set.

possible solution for the temporal extension could be to increase the difference between $Re_{\theta C}$ and $Re_{\theta t}$ to prevent the early increase in γ production triggered by the higher wake turbulence intensity.

7. CONCLUSIONS

A comprehensive study for unsteady prediction capabilities of recent transition models was conducted by utilizing the T106D-EIZ test case. This test case was selected because it is featuring an ultra-high-lift blade and exhibits a significant flow separation on the suction surface, which is temporarily influenced by the incoming wakes. Three different URANS based transition models were investigated to be compared against each other and the measurements. The main findings can be summarized as follows.

1) Results for the steady case with homogeneous inflow conditions showed for all three transition models under consideration here, qualitatively and quantitatively good agreement with the measured data.

2) For the unsteady results, good agreement with the measured time averaged isentropic Mach number and quasi wall shear stress data could, only be found for the integrative multimode transition model.

3) A closer analysis using time space diagrams for the wall shear stress compared against the measured quasi wall shear stress was undertaken. A temporarily too short but over the blade surface too long separation region for the two $\gamma - Re_{\theta t}$ transition models was detected.

4) A new method for analyzing time resolved boundary layers was used to deliver an explanation for the observed prediction deficit. Using so-called 3D time space diagrams for analysis it could be shown that the turbulence levels in front of the separation bubble exhibit particular differences, not in the freestream but in the near wall region.

5) Using the difference between $Re_{\theta C}$ and $Re_{\theta t}$ slightly upstream of the transition region, led to a proposal to adapt the $Re_{\theta C}$ correlation to overcome that shortening. Increasing the difference between the critical momentum thickness Reynolds number and the transition onset Reynolds number should deliver better results, which is studied in an ongoing investigation.

But there are still some open topics to be investigated in future research :
The reduced bar pitch leads to a higher number of bar wakes per blade pitch, which may have an influence on transition phenomena on the suction surface.
For the $\gamma - Re_{\theta t}$ cases the transition model was also applied for the bar surface in contrast to fully turbulent treatment for the multimode model case. This generated higher turbulence intensity, within the bar wakes, forcing an earlier transition by the $\gamma - Re_{\theta t}$ model as in case of the multimode model. For the multimode transition model, the turbulence level at the boundary edge is used to trigger the transition, this turbulence level is about 5% lower than compared to the $\gamma - Re_{\theta t}$ cases. Therefore it would be better to apply identical turbulence profiles at the inlet for a fair comparison of the transition models under consideration here.

8. ACKNOWLEDGMENTS

The authors wish to thank DLR Cologne, Institute of Propulstion Technology for provision of the flow solver TRACE and for their support. Also the authors wish to acknowledge the German D-Grid initiative for providing within the project AeroGrid (BMBF-01 IG 07006 E) cluster resources used for accomplishing this research. The measurements on the T106D-EIZ turbine cascade were performed and funded as part of the joint research program “Periodisch Instationäre Strömungen in Turbomaschinen” of the Deutsche Forschungsgemeinschaft (DFG).

[1] Mayle R. E., 1991, “The role of laminar-turbulent transition in gas turbine engines,” 91-GT-261,ASME Turbo Expo,Orlando,FL.

[2] Schlichting H., and Gersten K., 2006, Grenzschicht-Theorie, Springer-Verlag Berlin Heidelberg, 10. Überarbeitete Auflage.

[3] Stadtmüller P., and Fottner L., 2001, “A Test Case For the Numerical Investigation of Wake Passing Effects on a Highly Loaded LP Turbine Cascade Blade,” 2001-GT-0311, ASME Turbo Expo, New Orleans, LA, USA.

[4] Kelterer M. E., Burgstaller R., and Sanz W., 2011, “Application of the gamma-Re_theta transition model to transitional flow,” Proceedings of the 10th International Symposium on Experimental and Computational Aerothermodynamics of Internal Flows.

[5] Kožulović D., 2007, “Modellierung des Grenzschichtumschlags bei Turbomaschinen-strömungen unter Berücksichtigung mehrerer Umschlagsarten,” Ruhr-Universität Bochum.

[6] Menter F. R., Langtry R. B., Likki S. R., Suzen Y. B., Huang P. G., and Völker S., 2004, “A Correlation-Based Transition Model Using Local Variables: Part I - Model Formulation,” GT2004-53452, ASME Turbo Expo, Wien, Österreich.

[7] Langtry R. B., Menter F. R., Likki S. R., Suzen Y. B., Huang P. G., and Völker S., 2004, “A Correlation-Based Transition Model Using Local Variables: Part II - Test Cases and Industrial Applications,” GT2004-53454, ASME Turbo Expo, Wien, Österreich.

[8] Malan P., 2009, “Calibrating the gamma-Re_theta_t Transition Model for Commercial CFD,” 47th AIAA Aerospace Sciences Meeting.

[9] Crank J., and Nicolson P., 1996, “A Practical Method for Numerical Evaluation of Solutions of Partial Differential Equations of the Heat Conduction Type,” Advances in Computational Mathematics, **6**, pp. 207–226.

[10] Jameson A., 1991, “Time Dependent Calculations Using Multigrid with Applications to Unsteady Flows Past Airfoils and Wings,” AIAA 91-1596, AIAA 10th CFD Conference, Honolulu, HI, USA.

[11] Kato M., and Launder B. E., 1993, “The Modelling of Turbulent Flow Around Stationary and Vibrating Square Cylinders,” 9th Turbulent Shear Flow Symposium, Kyoto, Japan.

[12] Durbin P. A., and Peterson-Reif B. A., 2001, Statistical Theory and Modeling for Turbulent Flows, John Wiley & Sons, Chichester, Großbritannien.

[13] Kožulović D., Röber T., Kügeler E., and Nürnberger D., 2004, “Modifications of a Two-Equation Turbulence Model for Turbomachinery Fluid Flows,” Deutscher Luft- und Raumfahrtkongress, Dresden.

[14] Engel K., 1997, “Numerische Simulation der instationären Strömung in Turbomaschinen-komponenten,” Universität Gesamthochschule Essen.

[15] Eulitz F., 2000, “Numerische Simulation und Modellierung der instationären Strömung in Turbomaschinen,” Ruhr-Universität Bochum.

[16] Kožulović D., Röber T., and Nürnberger D., 2007, “Application of a Multimode Transition Model to Turbomachinery Flows,” 7th European Conference on Turbomachinery, Athen, Griechenland.

[17] Langtry R. B., 2006, “A Correlation-Based Transition Model using Local Variables for Unstructured Parallelized CFD codes.”

[18] Langtry R., and Menter F., 2009, “Correlation-Based Transition Modeling for Unstructured Parallelized Computational Fluid Dynamics Codes,” AIAA Journal 2009, **47**, pp. 2894–2906.

[19] Schwarze M., and Niehuis R., 2010, “Numerical Simulation of a Highly Loaded LPT Cascade With Strong Suction Side Separation Under Periodically Unsteady Inflow Conditions,” GT2010-22363, ASME Turbo Expo, Glasgow, UK.

[20] Yang H., Röber T., and Kožulović D., 2007, “Hybrid-Grid Simulation of Unsteady Wake-Boundary Layer Interaction on a High Lift Low Pressure Turbine Airfoil,” GT2007-28111, ASME Turbo Expo, Montreal, Kanada.

[21] Yang H., Nürnberger D., and Kersken H.-P., 2006, “Toward Excellence in Turbomachinery Computational Fluid Dynamics: A Hybrid Structured-Unstructured Reynolds-Averaged Navier-Stokes Solver,” Journal of Turbomachinery, **128**(4), pp. 390–402.

[22] Yang H., Nürnberger D., and Weber A., 2002, “A Conservative Zonal Approach with Applications to Unsteady Turbomachinery Flows,” DGLR-JT2002-073, DGLR Jahrestagung, Stuttgart.

[23] Stadtmüller P., Fottner L., and Fiala A., 2000, “Experimental and Numerical Investigation of Wake-Induced Transition on a Highly Loaded LP Turbine at Low Reynolds Numbers,” GT2000-0269, ASME Turbo Expo, München.